Evidence for Plasticity and Structural Mimicry at the Immunoglobulin Light Chain-Protein L Interface

Marc Graille, Steven Harrison, Matthew P Crump, Stuart C Findlow, Nicholas G Housden, Bruno H Muller, Nicole Battail-Poirot, Geneviève Sibaï, Brian J Sutton, Michael J Taussig, et al.

THE JOURNAL OF BIOLOGICAL CHEMISTRY
Vol. 277, No. 49, Issue of December 6, pp. 47500–47506, 2002

Printed in U.S.A.

Evidence for Plasticity and Structural Mimicry at the Immunoglobulin Light Chain-Protein L Interface*

Received for publication, June 19, 2002, and in revised form, September 4, 2002
Published, JBC Papers in Press, September 8, 2002, DOI 10.1074/jbc.M206105200

Marc Graille‡, Steven Harrison§, Matthew P. Crump§¶, Stuart C. Findlow§, Nicholas G. Housden§, Bruno H. Muller‖, Nicole Battail-Poirot, Geneviève Sibaï**, Brian J. Sutton‡‡, Michael J. Taussig§§, Colette Jolivet-Reynaud**, Michael G. Gore§¶ ¶¶, and Enrico A. Stura‡‖‖**

*From the ‡Laboratoire de Structure des Protéines and ‖UMR Commissariat à l'Energie Atomique (CEA)/bioMérieux, Département d'Ingénierie et d'Etudes des Protéines (DIEP), Commissariat à l'Energie Atomique, Centre d'Etudes de Saclay, 91191 Gif-sur-Yvette, France, the §Department of Biochemistry, Institute of Biomolecular Sciences, University of Southampton, Bassett Crescent East, Southampton SO16 7PX, United Kingdom, **bioMérieux, Département R & D Immunoessais et Protéomique, 69280 Marcy l'Étoile, France, the ‡‡Randall Centre, King's College London, Guy's Campus, London SE1 1UL, United Kingdom, and the §§Technology Research Group, The Babraham Institute, Babraham, Cambridge CB2 4AT, United Kingdom*

The multidomain bacterial surface protein L (PpL) is a virulence factor expressed by only 10% of *Peptostreptococcus magnus* strains, and its expression is correlated with bacterial vaginosis. The molecular basis for its ability to recognize 60% of mammalian immunoglobulin light chain variable regions (V_L) has been described recently by x-ray crystallography, which suggested the presence of two V_L binding sites on each protein L domain (Graille, M., Stura, E. A., Housden, N. G., Beckingham, J. A., Bottomley, S. P., Beale, D., Taussig, M. J., Sutton, B. J., Gore, M. G., and Charbonnier, J. (2001) *Structure* 9, 679–687). Here, we report the crystal structure at 2.1 Å resolution of a protein L mutant complexed to an Fab′ fragment with only 50% of the V_L residues interacting with PpL site 1 conserved. Comparison of the site 1 interface from both structures shows how protein L is able to accommodate these sequence differences and therefore bind to a large repertoire of Ig. The x-ray structure and NMR results confirm the existence of two V_L binding sites on a single protein L domain. These sites exhibit a remarkable structural mimicry of growth factors binding to their receptors. This could explain the protein L superantigenic activity on human B lymphocytes.

Gram-positive bacterial proteins that interact with immunoglobulins have been widely studied and utilized in immunology and biotechnology. Among the best known are *Staphylococcus aureus* protein A (SpA)[1] (1), streptococcal protein G (SpG) (2), and *Peptostreptococcus magnus* protein L (PpL) (3). They contain from two to five successive and highly homologous Ig-binding domains and recognize distinct regions on a wide portion of Ig. Protein L, a surface protein from *Peptostreptococcus magnus*, is 76–106 kDa in size and contains four to five (depending on the strain) highly homologous consecutive extracellular domains (4, 5). It binds with high affinity and high specificity to mammalian κ light chain variable ($V_L\kappa$) regions (6, 7). Although expressed by a minority of *P. magnus* strains, PpL appears to be a virulence factor because its presence is correlated with enhanced vaginal colonization (8) and the concomitant occurrence of bacterial vaginosis (9). PpL, like SpA and SpG, is an important tool for purification, recognition, and removal of immunoglobulins, but it has a different and unique specificity. SpA and SpG domains recognize a common site at the interface between the C_H2 and C_H3 domains on the Fc of IgG (Fcγ) (10, 11), but they also interact with functionally distinct regions on the Fab portion of particular Ig families or subclasses (SpA does not bind to most IgG3, whereas SpG does) (12, 13). SpG recognizes the Fab portion through binding to the C_H1 domain of IgG, whereas SpA interacts with the V_H domain on 12% of mouse and 50% of human Fv fragments. Although these two latter interactions have relatively low affinity (K_d of 200 nM), they have been used in specific cases for Fab purification and phage library validation. PpL does not share Fc binding ability with SpA and SpG, but its high affinity (K_d of 1 nM) for the variable light chain regions of more than two thirds of mouse and ~50% of human Ig, irrespective of their class, makes it particularly interesting for the purification of Fab fragments and single chain antibodies (scFv).

To understand better how PpL can bind a large population of light chains, we recently reported the crystal structure of the complex between a PpL single domain and a human Fab (14). Surprisingly, in this structure the PpL domain is sandwiched between two antibody light chains in a manner reminiscent of cytokines binding to their receptors at the cell surface (15–17).

* Work at The Babraham Institute is supported by the Biotechnology and Biological Sciences Research Council (BBSRC). The costs of publication of this article were defrayed in part by the payment of page charges. This article must therefore be hereby marked "*advertisement*" in accordance with 18 U.S.C. Section 1734 solely to indicate this fact.

The atomic coordinates and structure factors (code 1MHH) have been deposited in the Protein Data Bank, Research Collaboratory for Structural Bioinformatics, Rutgers University, New Brunswick, NJ (http://www.rcsb.org/).

¶ These authors were recipients of Wellcome Trust Grant 055640/Z/98/Z/ST/RC and Biotechnology and Biological Sciences Research Council Grants E10136, E15767, and E11896.

¶¶ To whom correspondence may be addressed. Tel.: 44-23-8059-4313; Fax: 44-23-8059-4459; E-mail: M.G.Gore@soton.ac.uk.

‖‖ To whom correspondence may be addressed. Tel.: 33-01-6908-4302; Fax: 33-01-6908-9071; E-mail: estura@cea.fr.

[1] The abbreviations used are: SpA, *Staphylococcus aureus* protein A; SpG, streptococcal protein G; PpL, *Peptostreptococcus magnus* protein L; V_L, variable light chain region; V_H, variable heavy chain region; C_L, constant light chain region; C_H, constant heavy chain region; Fv, variable fragment; Fc, constant fragment; PpL_{wt}, wild type protein L domain; PpL_{D55A}, protein L domain containing the Asp to Ala substitution at position 55; MPEG 5000, methoxypolyethylene glycol 5000; rmsd, root mean square deviation; TROSY, transverse relaxation optimized spectroscopy; HSQC, heteronuclear single quantum correlation.

From the two sites identified, only site 1 was already documented (18–20). To investigate the functional relevance of site 2, we have designed a PpL mutant (PpL D55A; hereafter PpL_{D55A}) where substitution of Asp-55 by Ala should disrupt a salt bridge and a hydrogen bond that was believed to be crucial for the interaction with PpL site 2. Thus, the PpL_{D55A} mutant should retain only site 1 binding for V_L. This mutant was built on the Y64W template, where Trp-64 is an efficient fluorescent probe to measure K_d by stopped flow methods (20).

Here, we present the complex between the PpL_{D55A} mutant and a mouse Fab′ fragment bearing a $V_L\kappa9$ region to 2.1Å resolution. The structure shows how PpL is able to accommodate differences in light chain sequences. The PpL_{D55A} mutant indeed shows a single binding mode in the crystal. To confirm the relevance of the second site in solution, we have studied the interaction between V_L chains and different PpL domains by heteronuclear NMR spectroscopy. Finally, we compare the residues involved in the first and second interfaces and reveal a strong homology between the two PpL interaction patches.

EXPERIMENTAL PROCEDURES

Cloning and Nucleotide Sequencing of 19D9D6 Antibody Heavy and Light Chains—Cloning of the 19D9D6 antibody (IgG1,κ) light chain was performed by standard methodology using classical PCR amplification as described previously (21). The cDNA encoding the Fd domain of the 19D9D6 antibody was obtained using the rapid amplification of cDNA ends (RACE) method, as described previously (22). The PCR products were obtained using the *Taq* DNA polymerase (Amersham Biosciences) and directly ligated into the pCR®2.1 cloning vector using a TA cloning kit (Invitrogen) according to the manufacturer's instructions. The sequences of cloned DNA were determined by sequencing on an ABI 310 automatic sequencer using a Dye Terminator Cycle Sequencing Ready Reaction Kit (Applied Biosystems).

Antibody Fragment Generation—The antibody 19D9D6 (IgG1,κ) was produced *in vitro* and purified as follows (23). Briefly, the supernatant was diluted 1:2 (v/v) in a high salt buffer, then loaded on a protein A column (Amersham Biosciences) and eluted at pH 6.0, following the manufacturer's instructions.

The $F(ab')_2$ fragment was obtained by proteolytic cleavage of the IgG by pepsin. The purified IgG was mixed with pepsin-agarose in an acidic buffer and digested for 1.5 h at 37 °C. The pepsin-agarose was then removed by centrifugation. The $F(ab')_2$ fragment was recovered in the supernatant and further purified by size exclusion chromatography on a Superdex 200 column (Amersham Biosciences). The Fab′ fragment was obtained by reduction with β-mercaptoethanol and blockage of the corresponding free cysteine residues with iodoacetamide. The Fab′ was further purified by size exclusion chromatography on Superdex 200.

Mutagenesis and Purification of the PpL_{D55A} and PpL_{D55N} Domains—The PpL_{D55A} and PpL_{D55N} mutants were made by mutating residue 55 on the Y64W or wild type template DNA (20) using the antisense primers 5′-TGC TAA TAA **AGC** TGC ATA TCT-3′ and 5′-TTT TGC TAA TAA **GTT** TGC ATA TCT GTA-3′, respectively. The sites of the mutations are shown in *boldface*. Mutations were confirmed by DNA sequencing using the Sequenase 2.2 DNA sequencing kit (USB Corporation). Proteins were purified as PpL_{wt} as described previously (24).

Preparation of ^{15}N-Labeled PpL Domains—Proteins labeled with the ^{15}N isotope were prepared by preculturing appropriately transformed *Escherichia coli* (JM103) in LB liquid media. Cells were harvested and resuspended in M9 minimal media supplemented with NH_4Cl (^{15}N), glucose, thiamine, $MnCl_2$, and $FeCl_3$. Protein expression was induced by addition of isopropyl-1-thio-β-D-galactopyranoside (IPTG) after a 1 h incubation at 37 °C with shaking. Cells were harvested after a further 18-h incubation, whereupon ^{15}N-labeled PpL was purified as described in Ref. 24.

NMR—All NMR spectra were recorded on a Varian Inova 600 MHz NMR spectrometer. Solution conditions for PpL_{wt} and PpL_{D55N} were 20 mM deuterated sodium acetate, pH 5.5, and 1 mM NaN_3 in 95:5% H_2O/D_2O. PpL_{wt} and PpL_{D55N} concentrations were typically 300 μM, and $V_L\kappa1$ was added to the solutions to give final solution concentrations of 150 and 300 μM $V_L\kappa1$ (2:1 and 1:1 $PpL{\cdot}V_L$). ^{1}H-^{15}N correlation spectra were recorded using the TROSY pulse sequence provided by Lewis Kay, and measuring times were 30 min for control spectra and 4 h for the $PpL{\cdot}V_L$ complexes.

Crystallization—The Fab′ 19D9D6·PpL_{D55A} complex was prepared in solution before the crystallization trials by mixing 18 μl of Fab′ 19D9D6 (6 mg/ml) with 4 μl of PpL_{D55A} (16 mg/ml). Crystals were grown by vapor diffusion at room temperature in sitting drops by mixing 3 volumes of a reservoir solution containing 10% (w/w) MPEG 5000, 100 mM sodium acetate, pH 4.5, with 4 volumes of the protein solution. Crystals suitable for data collection were enlarged by using streak seeding followed by macroseeding (25). For data collection, crystals were transferred into a cryo-solution containing 5 μl of ethylene glycol, 3 μl of 50% (w/w) MPEG 5000, and 10 μl of 3 mM $ZnCl_2$, 3 mM $CdCl_2$, 100 mM sodium cacodylate, pH 6.5, and 50% (w/w) MPEG 5000. Two data sets were recorded at 100 K from isomorphous crystals to 2.6Å and later to 2.1Å resolution on ID14-EH2 and ID14-EH4 beamlines respectively (European Synchrotron Radiation Facility, Grenoble, France). Data were processed using the HKL package (26). Crystals belong to the orthorhombic space group $P2_12_12_1$. Statistics are summarized in Table I.

Structure Determination and Refinement—The 25–2.6 Å data set was used to solve the structure by the molecular replacement method with the program AMORE (27). Using the coordinates from the variable (V_L/V_H) and constant (C_L/C_H1) regions of the uncomplexed Fab′ 19D9D6 structure (28) as independent search models, the two Fab′ molecules present in the asymmetric unit were correctly positioned (Table I). Any attempts to position the two PpL molecules were unsuccessful. After an initial refinement of this model, σ_A-weighted $2F_o - F_c$ and $F_o - F_c$ electron density maps were analyzed with the program TURBO (29). These maps show electron density corresponding to a single PpL domain in the vicinity of the V_L region from both Fab′ molecules. The PpL domains were thus fitted into these maps by superimposing on both Fab′ molecules the previously solved structure of the complex between a human Fab and the PpL_{wt} domain (14) with the program ALIGN (30). The two Fab′·PpL_{D55A} complexes present in the asymmetric unit were first refined within the 25–2.7 Å resolution range with non-crystallographic symmetry restraints of 100 kcal/mol/Å^2 applied to the whole model with the exception of the domains involved in the interfaces and finally from 20 to 2.1 Å resolution without non-crystallographic symmetry restraints. The structure was refined with the program CNS (31), and the model was rebuilt in TURBO. Statistics for the structure determination are listed in Table I. The final model contains 994 residues, 733 water molecules, and 2 ethylene glycol molecules from the cryo-solution. Detectable residues range from 20 to 82 for the first PpL_{D55A} domain and from 20 to 81 for the second PpL_{D55A} domain. As observed for all PpL domain structures solved to date (14, 32, 33), the 19 N-terminal residues are disordered and thus absent from the final model. With the exception of small loops from the C_H1 region and to a lesser extent the complementarity determining region L1, the final model is well defined in the electron density map.

Structure Analysis—All but one residue from each complex display main chain dihedral angles that fall within allowed regions of the Ramachandran plot as defined by the program PROCHECK (34). The only exception is Ala L51 from the L2 hypervariable loop, which has been found to adopt unfavorable conformations in many crystal structures of Fab fragments. The V_L conformation is unchanged between the two Fab′ molecules with a root mean square deviation (rmsd) of 0.21Å over 430 backbone atoms as calculated by the program ALIGN (30). Similarly, both PpL_{D55A} domains superimpose well on each other with an rmsd of 0.42Å over 240 backbone atoms with the largest shift found for the loop connecting β-strands 3 and 4, which is less well defined in electron density. The PpL_{D55A} domain assumes the same three-dimensional structure as the PpL_{wt} domain (14), and the PpL_{Y64W} domain solved to 1.7Å resolution (Y47W according to O'Neill numbering (33)) with rmsd of 0.5Å over 230 backbone atoms for each case.

Residues were considered to be at the interface when they fulfilled two conditions. 1) At least one van der Waals contact (cutoff = 4Å; calculated with program CONTACT from the CCP4 package (35)) is made with a residue from the partner molecule. 2) Either the residue is fully buried upon complexation, or it buries at least 20 Å^2 in the interface. The solvent-accessible surface areas were estimated with the program AREAIMOL from CCP4 (35). Hydrogen bond distances were calculated using the program CONTACT (35) with a maximum distance cut-off of 3.4 Å and defined according to the criteria of McDonald and Thornton (36).

RESULTS AND DISCUSSION

Overall Structure of the Fab′ 19D9D6·PpL_{D55A} Complex—The Fab′ 19D9D6 bears a V_L chain belonging to the murine κ9 family, which is related to the human κ4 family. The asymmetric unit contains two Fab′ 19D9D6·PpL_{D55A} complexes related

TABLE I
Data collection, phasing and refinement statistics

Data collection

Category	1st data set	2nd data set
Resolution (Å) (Last shell)	25–2.6 (2.68–2.6Å)	20–2.1 (2.16–2.1Å)
Unique reflections	35,392	69,723
Redundancy	3.13 (3.27)	6.77 (5.86)
I/	12 (2.35)	26.6 (3.5)
R_{sym} (%)	9.7 (61.7)	6.7 (41.7)
Completeness (%)	96.9 (99.3)	97.6 (85)
Space group	$P2_12_12_1$	$P2_12_12_1$
Unit cell parameters	a = 77.53 Å, b = 100.61 Å, c = 148.95 Å	a = 78.49 Å, b = 100.96 Å, c = 149.15 Å

Molecular replacement

Category	1st data set	2nd data set
Resolution (Å)	25–4.0	
Correlation coefficient (%)	63.3 (50.8)[a]	

Refinement

Category	1st data set	2nd data set
Resolution (Å)		20–2.1
R_{work} (%)[b]		19.7
R_{free} (%)[b,c]		24.7
R.m.s. deviations:		
Bonds (Å)		0.005
Angles (°)		1.300
Averaged B-factor (Å^2)		40.4
Luzzati coordinates error (Å)		0.24

[a] Correlation coefficient for the next highest solution is indicated in bracket.
[b] R_{work} and R_{free} values in the last shell (2.11–2.10Å) are respectively 22.3 and 23.6%.
[c] Value of R_{free} calculated for 5% randomly chosen reflections not included in the refinement.

by non-crystallographic symmetry. The two complexes superimpose on each other with a rmsd of 0.6 Å over 690 backbone atoms with the largest shift observed for the PpL helix with no consequences on the interface. In contrast with the PpL_{wt} domain which contacts two Fab molecules in the complex with human Fab 2A2 (14), the PpL_{D55A} mutant binds to only one Fab′ molecule. This interaction occurs via PpL site 1 on the opposite side of the domain from the D55A mutation.

Comparison between the PpL·$V_L\kappa9$ and $V_L\kappa1$ Interfaces—The interactions made by PpL_{D55A} with the V_L region of Fab′ 19D9D6 (murine $V_L\kappa9$) are different from those observed for Fab 2A2·PpL_{wt} complex (human $V_L\kappa1$) as a result of differences in their κ chain sequences. Six of the twelve V_L residues involved in the Fab 2A2 $V_L\kappa1$·PpL_{wt} complex are different in the $V_L\kappa9$ sequence. However, their chemical character is conserved, *e.g.* Ser L5 is Thr in $V_L\kappa1$, Ala L12 is Ser, Val L13 is Ala, Lys L18 is Arg, Ser L22 is Thr, and Lys L24 is Arg (Fig. 1*A*). These changes do not affect the overall structure of the complexes which superimpose well (rmsd of 0.6 Å over 660 backbone atoms). The PpL strand β2 and the V_L β-strand A are anti-parallel and are connected through hydrogen bonds between main chain atoms from both partners forming a β-zipper interaction. This extends a β-sheet from the V_L region into the PpL β-sheet as was observed in the Fab 2A2·PpL_{wt} structure (14). Although the overall binding mode is unchanged, several interactions are different. Only 20 residues (11 from Fab′ 19D9D6 and 9 from PpL_{D55A}) are involved in pairwise interactions in this structure compared with 25 in the $V_L\kappa1$ complex (13 from the Fab 2A2 and 12 from PpL_{wt}). With the exception of Glu L17, which is an aspartate in Fab 2A2, all of these positions were already identified (Fig. 1, *A* and *B*). Four hydrogen bonds out of six are common: three that mediate the formation of the β-zipper and one connecting PpL Tyr-53 hydroxyl to the Thr L20 carbonyl (Table II). This confirms that these hydrogen bonds between PpL and the V_L main chain are important for the recognition of a large population of $V_L\kappa$ regions in a sequence-independent manner.

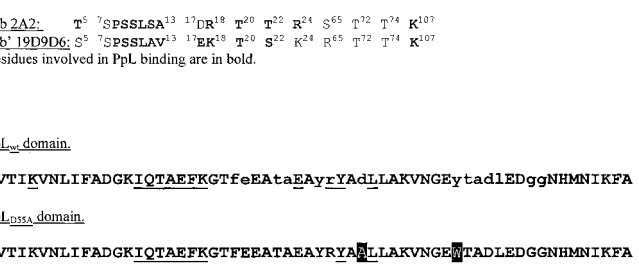

FIG. 1. **Residues involved in site 1 are *underlined*, those in site 2 are in *lower case*, and the arginine residue participating in both sites in the PpL_{wt} domain is in *lower case* and *underlined*.** The two mutated residues in the PpL_{D55A} domain are in *white*. *A*, sequence comparison of the residues involved in PpL binding from Fab 2A2 (human $V_L\kappa1$) and Fab′ 19D9D6 (murine $V_L\kappa9$). *B*, PpL residues involved in sites 1 and 2 binding in PpL_{wt} and PpL_{D55A} domains.

Surprisingly, although the serine L9 and L10 regions are conserved in Fab′ 19D9D6, the hydrogen bonds made from Ser L9 Oγ to Lys-40 N and from Ser L10 Oγ to Glu-38 Oε1 in the Fab 2A2·PpL_{wt} complex are absent in this structure because of the rotation of both serine side chains. Three additional hydrogen bonds compensate for this loss. These are created by the rearrangement of the N-terminal part of PpL strand β2 and of the linker region connecting the V_L to the C_L domain (residues L-106 to L-112). These have been found to be among the most flexible PpL and Fab′ segments. NMR studies have shown that PpL β2 has a faster average proton exchange rate than inner strands (β1 and β4) (32, 37). In the two crystal structures, this PpL segment adopts two alternative stable conformations (this study and Ref. 14). In the new conformation, the N-terminal portion of PpL strand β2 is closer to the V_L strand A and makes two additional hydrogen bonds. The first one connects the Ala L12 carbonyl to the PpL Thr-36 amide, thus extending the

TABLE II
Hydrogen bonds interactions in the V_L PpL_{D55A} interface

Hydrogen bonds conserved between the human $V_L\kappa1$ and murine $V_L\kappa9$ complexes are in bold.

V_L region	PpL_{D55A} domain	Distance	
		1st complex of the asymmetric unit	2nd complex of the asymmetric unit
		Å	
Ser L9 N	**O Glu-38**	**2.7**	**2.7**
Ser L10 O	**N Glu-38**	**3.0**	**3.1**
Ala L12 N	**O Thr-36**	**2.8**	**2.7**
Ala L12 O	N Thr-36	3.1	3.1
Lys L18 O	Nε2 Gln-35	2.9	2.8
Thr L20 O	**Oη Tyr-53**	**2.6**	**2.7**
Lys L107 Nζ	Oγ1 Thr-36	3.0	2.9

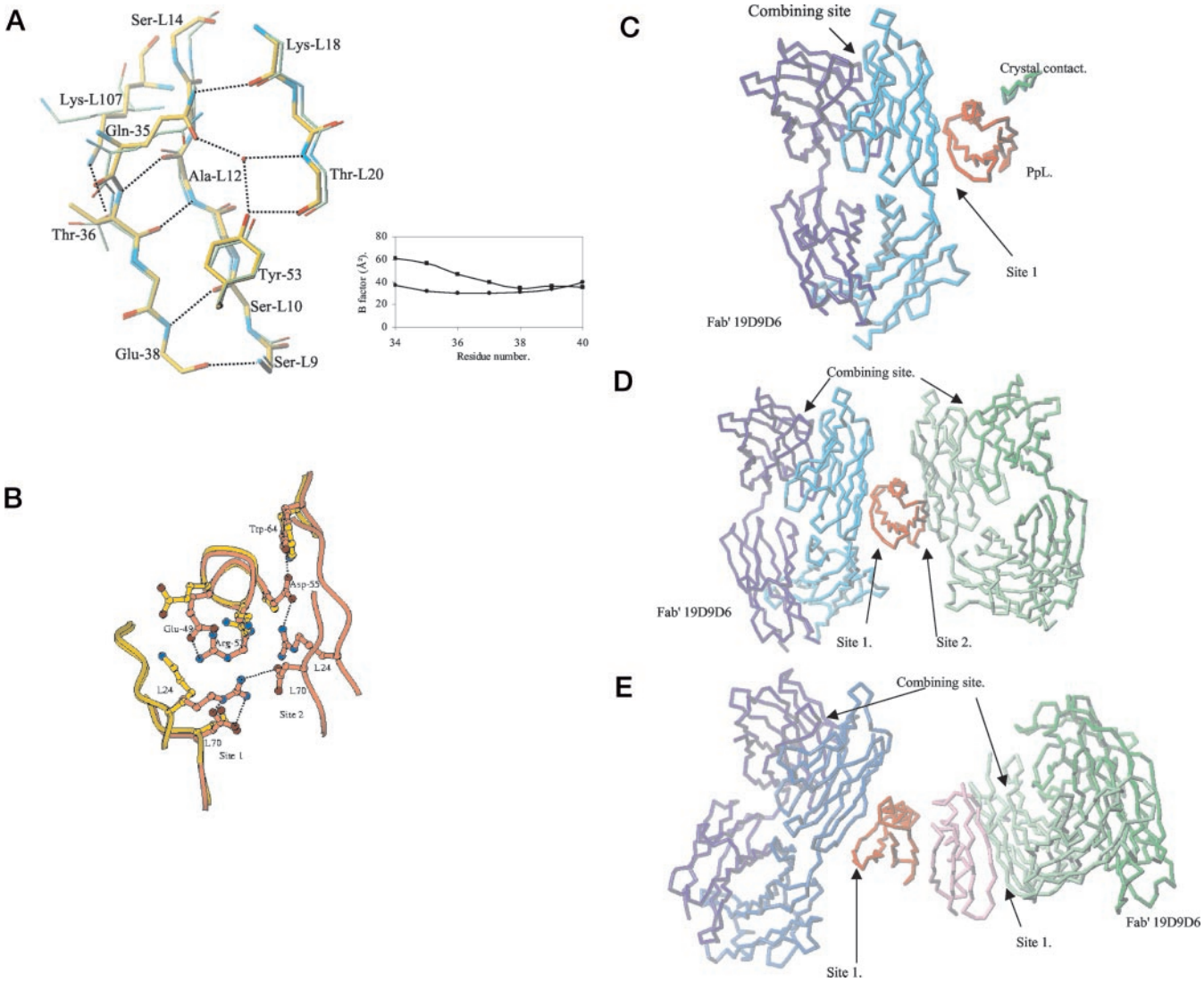

FIG. 2. **Differences at the first V_L-PpL interface.** *A*, comparison of binding to PpL site 1 in the Fab 2A2 and Fab′ 19D9D6 complexes. The Fab′ 19D9D6·PpL_{D55A} complex carbon atoms are shown in *yellow*, and those of the Fab 2A2-PpL_{wt} complex are *green*. For clarity, only selected side chains are shown. Hydrogen bonds identified in the Fab′ 19D9D6·PpL_{D55A} complex are depicted as *dashed lines*. *Inset*, comparison of the average crystallographic B factors for the main chain atoms of residues 34–40 from PpL strand β2. The two extra hydrogen bonds described for the $V_L\kappa9$·PpL_{D55A} complex (*circles*) compared with the $V_L\kappa1$·PpL_{wt} complex (*squares*) reduce the thermal agitation of PpL residues 34–36 relative to portions 37–40. *B*, superimposition of the Fab 2A2·PpL_{wt} structure (*pink*) on that of Fab′ 19D9D6 (*yellow*). Positions from the V_L regions are indicated by their number preceded by the letter L, and those from PpL are identified by their three letter code. The electrostatic interaction network implicated in the Fab 2A2·PpL_{wt} structure is depicted by *dashed lines*. *C*, schematic representation of the Fab′ 19D9D6·PpL_{D55A} complex with site 2 involved in minor crystal contact. *D*, schematic representation of the two-site complex formed between site 1 PpL mutants and the Fab′ 19D9D6. *E*, schematic representation of a PpL dimer binding two $V_L\kappa9$ through site 1. Site 2 is involved in dimer formation.

β-zipper interaction by a fourth hydrogen bond (Table II and Fig. 2*A*). The second links PpL Gln-35 $N_\epsilon2$ to the Lys L18 carbonyl. As a result, the N-terminal part of PpL strand β2 is more constrained than in the Fab 2A2·PpL_{wt} structure (Fig. 2*A*, *inset*). In addition, the movement of the main chain of Lys L107 from the V_L-C_L linker region combined with the rearrangement of its long side chain creates a hydrogen bond between Lys N_ζ and Thr-36 $O_\gamma1$.

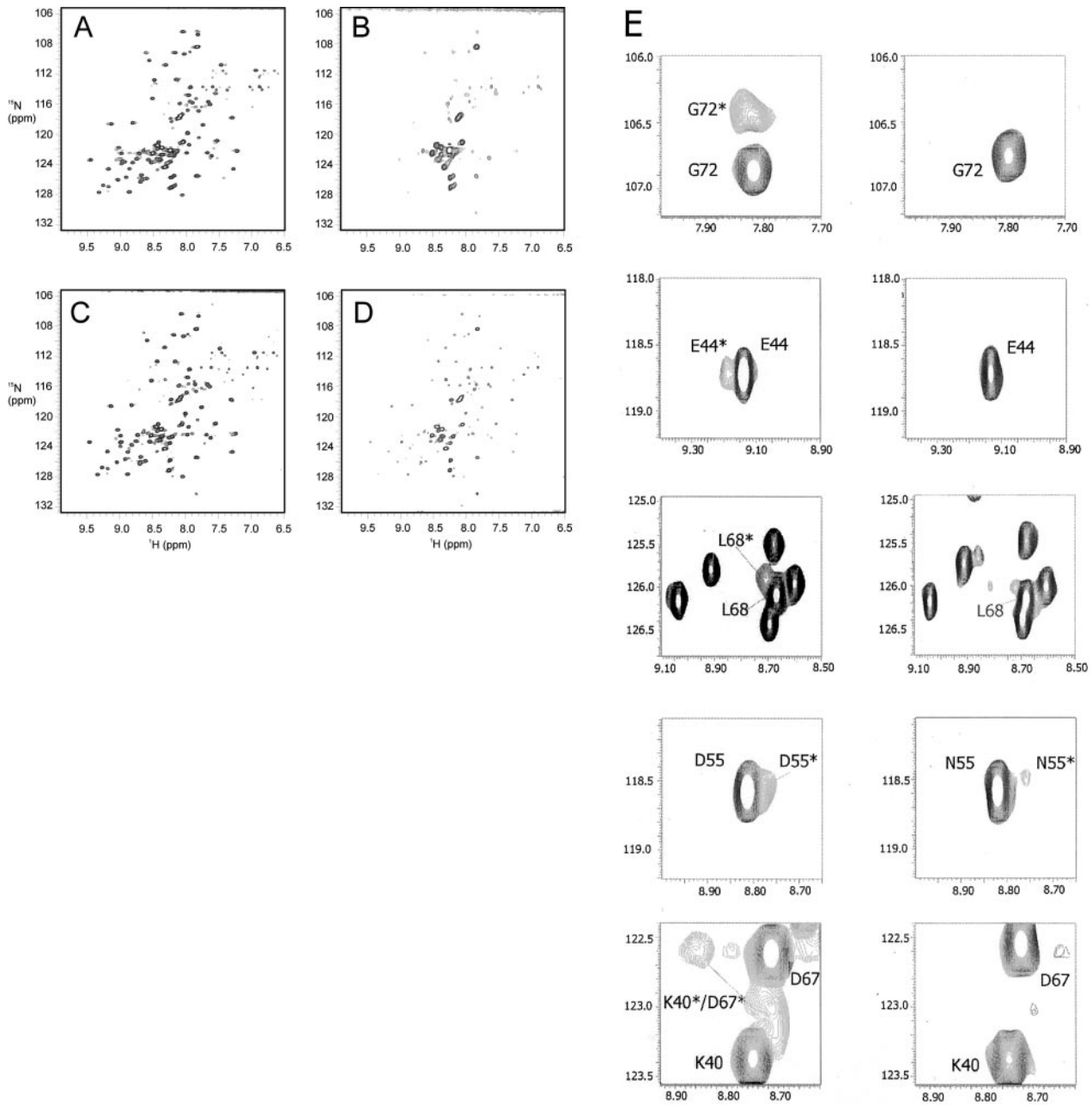

FIG. 3. **NMR.** Selected expansions from the TROSY-HSQC spectra of PpL·$V_L\kappa1$ titrations. *A*, PpL_{wt}·$V_L\kappa1$ at 2:1 stoichiometry. *B*, PpL_{wt}·$V_L\kappa1$ at 1:1 stoichiometry. *C*, PpL_{D55N}·$V_L\kappa1$ at 2:1 stoichiometry. *D*, PpL_{D55N}·$V_L\kappa1$ at 1:1 stoichiometry. *E*, peak expansions of individual ^{1}H-^{15}N correlations from the PpL_{wt} (*left*) and PpL_{D55N} (*right*) TROSY-HSQC spectra at 2:1 PpL-$V_L\kappa1$ molar ratio. An *asterisk* indicates peaks that are only visible in the PpL·$V_L\kappa1$ complex.

Some V_L positions (L5, L143 and L24) previously identified to contact PpL play no direct role in the 19D9D6 interface. First, at position L5, the change from Thr in Fab 2A2 to Ser in the Fab′ 19D9D6 eliminates a contact with Glu-49 mediated by the Thr Cγ1. Second, a difference in the V_L-C_L elbow angle (140° in Fab′ 19D9D6 *versus* 160° in Fab 2A2) eliminates the van der Waals interaction between position L143, a glutamate from the C_L domain, and Lys-24 Nζ from PpL. However, in another crystal form, as a result of a change in crystal packing, the V_L-C_L elbow angle of the same Fab′ complexed to another PpL mutant is 165°, and position L143 regains its role in site 1.[2] This suggests that this van der Waals interaction is of secondary importance for complex formation. At position L24, a Lys replaces an Arg. Arg L24 from site 1 in the Fab 2A2·PpL_{wt} complex is involved in van der Waals interaction with PpL Arg-52 and makes a salt bridge to V_L Asp L70 from another light chain bound to site 2 (Fig. 2*B*). In the Fab′ 19D9D6·PpL_{D55A} complex, the side chain of Lys L24 is flexible as shown by the absence of strong electron density and does not contact PpL. This is not due to the loss of site 2, because in the complex with another PpL mutant that binds to two V_L regions, the Lys L24 from the Fab′ 19D9D6 bound to site 1 does not contact the other Fab′ 19D9D6 bound to PpL site 2.[2] This results in a decrease in the buried area from 1300 Å^2 for PpL_{wt}·$V_L\kappa1$ to 1150 Å^2 for $V_L\kappa9$ at site 1.

In summary, although the two V_L regions crystallized in complex with PpL share only 50% sequence identity among the contact residues, the PpL·V_L interface is largely conserved. Amino acid differences, backbone movements, and side chain

[2] M. G. Gore, manuscript in preparation.

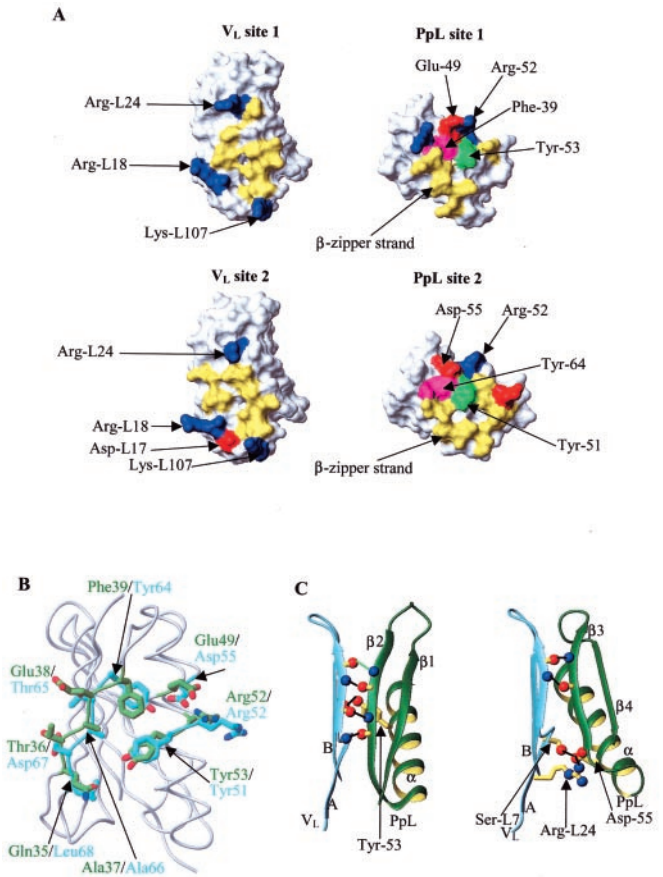

FIG. 4. **Structural resemblance between site 1 and site 2.** *A*, V_L (*left*) and PpL (*right*) surfaces involved in either site 1 (*top*) or site 2 (*bottom*). Positively and negatively charged residues are in *blue* and *red*, respectively (14). The other residues are in *yellow* with the exception of the matching hydrophobic residues, which are in *green* (PpL Tyr-51 and Tyr-53) or *magenta* (PpL Phe-39 and Tyr-64). The PpL domain is rotated by 180° relative to the V_L region, which has the same orientation in both cases. *B*, matching between PpL residues involved in site 1 (*green*) or in site 2 (*cyan*). *C*, β-zipper interactions involved in site 1 (*left*) and site 2 (*right*). Hydrogen bonds responsible for each interaction are depicted by *dotted lines*. The fourth main chain to main chain hydrogen bond highlighted by the present structure at site 1 is in *green*.

rearrangements modulate the overall interaction, but a conserved core of residues from both partners ensures the ability of PpL to maintain its interaction. This ensures recognition of as much as 50% of the human immunoglobulin repertoire, mainly because the β-zipper and Tyr-53 contact only V_L backbone atoms. Thus the interaction is sequence independent, and only light chains with an altered backbone conformation escape PpL recognition (*e.g.* $V_L\kappa 2$ and $V_L\lambda$).

Evidence for the Existence of Site 2 in Solution—In the structure presented here, the PpL region responsible for site 2 (strand β3 and one side of the α-helix) is mostly solvent exposed and is only involved in a minor crystal contact, showing that the mutagenesis has effectively targeted an important residue for site 2 (Fig. 2*C*). Thus, after the truncation of the Asp-55 side chain, this mutant is unable to interact through the large contact surface found in the Fab 2A2·PpL_{wt} complex but establishes instead a minor crystal contact. Other reasons could be advanced to explain the absence of site 2 interactions; first, it could be just a crystal contact, and second, it could be due to sequence differences between the V_L regions of Fab 2A2 and Fab′ 19D9D6. Both possibilities are dismissed by the analysis of the crystal packing of three other PpL mutants in complex with the same Fab′ (28). The two PpL mutant domains with intact site 2 (the modified residues Tyr to Phe at position 53 or Leu to His at position 57 are both in site 1) are sandwiched between two Fab′ 19D9D6 exactly as observed for the complex between human Fab 2A2 and PpL_{wt} (Ref. 14 and Fig. 2*D*). The third construct where residues Asp-55 and Leu-57 have been mutated to Ala and His, respectively, crystallizes in a different crystal form and binds to the Fab′ only through site 1 (Fig. 2*E*). This provides strong evidence to support the claim that the aspartic residue at position 55 plays a key role in site 2, and its replacement by an alanine is sufficient to disrupt this site.

To complement x-ray crystallographic data, we have used heteronuclear solution NMR spectroscopy to map the V_L binding site of PpL with human $V_L\kappa 1$ in combination with the TROSY method (38). Spectra obtained by this approach should allow a clearer observation of resonances in the complex with a gain in sensitivity compared with previous NMR studies (18). We have compared the chemical shifts induced on two different PpL domains, PpL_{wt} and PpL_{D55N} (but not PpL_{D55A} because of aggregation problems), upon V_L binding at two different PpL·$V_L\kappa 1$ ratios (2:1 and 1:1). At a 2:1 ratio, both PpL_{wt} and PpL_{D55N} ^1H-^{15}N HSQC spectra show a mixture of complexed and uncomplexed species as evident from the persistence of cross peaks at the native chemical shifts and the appearance of a set of weak and broad signals (Fig. 3, *A* and *C*). Upon continuation of the titration to a 1:1 stoichiometry, the PpL_{wt} spectrum becomes almost completely broadened out with the exception of intense signals from the N-terminal residues (Fig. 3*B*). This is consistent with the formation of a complex of larger molecular weight that does not involve the disordered N-terminal residues as seen by crystallography (14). Conversely, the equivalent PpL_{D55N} spectrum still displays visible backbone resonances at the 1:1 stoichiometry (Fig. 3*D*). This is a clear indication that the overall binding of PpL_{D55N} to $V_L\kappa 1$ chains has been reduced relative to PpL_{wt}.

For an analysis of the possible V_L binding sites on PpL, the PpL_{wt} and PpL_{D55N} spectra at 2:1 PpL·$V_L\kappa 1$ molar ratio proved to be the most useful (Fig. 3*E*). We have focused on some residues from PpL site 2 (Glu-44, Asp or Asn-55, Asp-67, Leu-68, and Gly-72). Whereas these residues in PpL_{wt} clearly show a set of weak shifted peaks associated with the main peaks (Fig. 3*E*, *left panel*), these weak peaks are largely absent in the PpL_{D55N} spectrum (Fig. 3*E*, *right panel*), although a small perturbation for both Asn-55 and Leu-68 is visible, indicating that some weaker association may persist at site 2.

The above NMR results clearly demonstrate different $V_L\kappa 1$ binding properties for PpL_{wt} and PpL_{D55N} domains. They also confirm the existence of site 2, which is weakened by the Asp-55 to Asn substitution (and most probably by the Asp to Ala). This raises the number of V_L binding sites on the whole PpL molecule from five to ten (or from four to eight, depending on the *P. magnus* strain). Since its discovery, PpL was considered to bear only one V_L binding site on each domain, and all the previous conclusions were based on this assumption. These new results are important and allow a more precise interpretation of the biological activity of PpL. Through these two sites, PpL is able to interact with many antibodies outside the antigen combining site in a manner reminiscent of SpG and SpA. As in the binding properties shown by SpA and SpG domains, dual site binding renders PpL inaccessible to antibodies, which may serve to effectively hide the bacterial protein and the bacterium from immune surveillance. What role this mechanism plays in the defense strategy of these bacteria remains to be established. However, like SpA, PpL can act as a B-cell superantigen through its Fab binding property, (39).

Structural Convergence between the Two V_L Binding Sites—In the Fab 2A2·PpL_{wt} complex, PpL contacts the same V_L stretch (L1 to L24; Figs. 1*B* and 4*A*) from both Fabs in the

ternary complex and buries a similar area (1300 $Å^2$ for site 1 and 1400 $Å^2$ for site 2) (Fig. 4*A*). Superimposition of the V_L region of the two Fabs in complex with PpL_{wt} brings both PpL sites into alignment, exposing a strong similarity between the two interfaces. Asp-55 overlies Glu-49, Tyr-53 maps on Tyr-51, Ala-37 on Ala-66, Arg-52 overlies itself, and the other corresponding residues have a matching chemical character (Fig. 4*B*). This includes Phe-39 that overlays Tyr-64, both of which have been mutated to Trp without affecting binding at either site (19, 28). The structural mimicry between the two interfaces is also found at the secondary structure level. Both PpL binding sites involve a whole β-strand and one side of an α-helix, although strand A from the V_L region is anti-parallel to PpL strand 2 (site 1) but parallel to PpL strand 3 (site 2) (Fig. 4*C*). These strand-to-strand interactions are of the β-zipper type with four hydrogen bonds made between site 1 of PpL_{D55A} and Fab′ 19D9D6 compared with only two hydrogen bonds formed between site 2 of PpL_{wt} and Fab 2A2. The superimposition can guide a program of mutagenesis to establish which residues found in a PpL domain are essential in each of the two closely related $V_L\kappa$ light chain binding sites and whether or not the two sites share critical residues.

It is surprising to find that the two sites appear not to be the result of gene duplication but the result of functionally driven structural convergence. Although such a strong structural mimicry has not been observed before, other molecules have developed two non-identical binding sites to the same target. The extracellular ligands of class 1 cytokine receptors, like human growth hormone (hGH) and erythropoietin (EPO) bind to their receptors divalently with a one ligand-two receptor stoichiometry (15–17). In the three cases, two different sites on the ligand contact similar regions of the receptors. However, in the case of hGH and EPO, the strong mimicry described above is not present. The PpL·V_L interactions better resemble the interaction of EPO with its receptor because of the lack of receptor-receptor contacts and the unequal affinities between the two binding sites (three orders of magnitude difference for EPO (40)). What are the consequences of a PpL domain binding to two B-cell receptors? Does the presence of a second binding site offer a biological advantage to a protein that already has up to five sequential Ig binding domains? In the case of EPO, it has been shown that not all dimerization will lead to activation (41). It is thus possible that a similarity may exist between the manner in which PpL interacts with B cell receptors and the way that cytokines interact with their receptors. From a structural point of view, a flexible string of domains may not give a precise signal in the same way that single-domain PpL-dimerized receptors could. The analogy is very suggestive and merits further investigation.

In conclusion, these results enhance our knowledge of the mechanism adopted by PpL to interact with almost half of the human B cell repertoire overcoming sequence variation at the recognized V_L positions. By combination of x-ray crystallography and NMR methods, we confirm the existence of two independent, simultaneous V_L binding sites on a single PpL domain.

Acknowledgments—We thank the local contacts from beamlines ID14-EH2 and ID14-EH4 at the European Synchrotron Radiation Facility (ESRF). We are indebted to Drs. F. A. Rey and S. Bressanelli for help during data collection at ESRF. We thank Dr. B. Gilquin and Prof. A. Ménez for continuous encouragement and Drs. M-H. Le Du and I. Krimm for help in preparation of this manuscript.

REFERENCES

1. Langone, J. J. (1982) *Adv. Immunol.* **32,** 157–252
2. Bjorck, L., and Kronvall, G. (1984) *J. Immunol.* **133,** 969–974
3. Bjorck, L. (1988) *J. Immunol.* **140,** 1194–1197
4. Murphy, J. P., Duggleby, C. J., Atkinson, M. A., Trowern, A. R., Atkinson, T., and Goward, C. R. (1994) *Mol. Microbiol.* **12,** 911–920
5. Kastern, W., Sjobring, U., and Bjorck, L. (1992) *J. Biol. Chem.* **267,** 12820–12825
6. Akerstrom, B., and Bjorck, L. (1989) *J. Biol. Chem.* **264,** 19740–19746
7. Nilson, B. H., Solomon, A., Bjorck, L., and Akerstrom, B. (1992) *J. Biol. Chem.* **267,** 2234–2239
8. Ricci, S., Medaglini, D., Marcotte, H., Olsen, A., Pozzi, G., and Bjorck, L. (2001) *Microb. Pathog.* **30,** 229–235
9. Kastern, W., Holst, E., Nielsen, E., Sjobring, U., and Bjorck, L. (1990) *Infect. Immun.* **58,** 1217–1222
10. Deisenhofer, J. (1981) *Biochemistry* **20,** 2361–2370
11. Sauer-Eriksson, A. E., Kleywegt, G. J., Uhlen, M., and Jones, T. A. (1995) *Structure* **3,** 265–278
12. Derrick, J. P., and Wigley, D. B. (1992) *Nature* **359,** 752–754
13. Graille, M., Stura, E. A., Corper, A. L., Sutton, B. J., Taussig, M. J., Charbonnier, J. B., and Silverman, G. J. (2000) *Proc. Natl. Acad. Sci. U. S. A.* **97,** 5399–5404
14. Graille, M., Stura, E. A., Housden, N. G., Beckingham, J. A., Bottomley, S. P., Beale, D., Taussig, M. J., Sutton, B. J., Gore, M. G., and Charbonnier, J. (2001) *Structure* **9,** 679–687
15. Cunningham, B. C., Ultsch, M., De Vos, A. M., Mulkerrin, M. G., Clauser, K. R., and Wells, J. A. (1991) *Science* **254,** 821–825
16. de Vos, A. M., Ultsch, M., and Kossiakoff, A. A. (1992) *Science* **255,** 306–312
17. Syed, R. S., Reid, S. W., Li, C., Cheetham, J. C., Aoki, K. H., Liu, B., Zhan, H., Osslund, T. D., Chirino, A. J., Zhang, J., Finer-Moore, J., Elliott, S., Sitney, K., Katz, B. A., Matthews, D. J., Wendoloski, J. J., Egrie, J., and Stroud, R. M. (1998) *Nature* **395,** 511–516
18. Wikstrom, M., Sjobring, U., Drakenberg, T., Forsen, S., and Bjorck, L. (1995) *J. Mol. Biol.* **250,** 128–133
19. Beckingham, J. A., Bottomley, S. P., Hinton, R., Sutton, B. J., and Gore, M. G. (1999) *Biochem. J.* **340,** 193–199
20. Beckingham, J. A., Housden, N. G., Muir, N. M., Bottomley, S. P., and Gore, M. G. (2001) *Biochem. J.* **353,** 395–401
21. Bettsworth, F., Monnet, C., Watelet, B., Battail-Poirot, N., Gilquin, B., Jolivet, M., Menez, A., Arnaud, M., and Ducancel, F. (2001) *J. Mol. Recognit.* **14,** 99–109
22. Ruberti, F., Cattaneo, A., and Bradbury, A. (1994) *J. Immunol. Methods* **173,** 33–39
23. Jolivet-Reynaud, C., Dalbon, P., Viola, F., Yvon, S., Paranhos-Baccala, G., Piga, N., Bridon, L., Trabaud, M. A., Battail, N., Sibai, G., and Jolivet, M. (1998) *J. Med. Virol.* **56,** 300–309
24. Bottomley, S. P., Beckingham, J. A., Murphy, J. P., Atkinson, M., Atkinson, T., Hinton, R. J., and Gore, M. G. (1995) *Bioseparation* **5,** 359–367
25. Stura, E. A., and Wilson, I. A. (1991) *J. Cryst. Growth* **110,** 270–282
26. Otwinowski, Z., and Minor, W. (1997) *Methods Enzymol.* **276,** 307–326
27. Navaza, J. (1994) *Acta Crystallogr. Sect. A* **50,** 157–163
28. Stura, E. A., Graille, M., Housden, N. G., and Gore, M. G. (2002), *Acta Crystallogr. Sect. D Biol. Crystallogr.* **58,** 1744–1748
29. Roussel, A., and Cambillau, C. (1989) *Silicon Graphics Geometry Partner Directory*, pp. 77–78, Silicon Graphics, Mountain View, CA
30. Satow, Y., Cohen, G. H., Padlan, E. A., and Davies, D. R. (1986) *J. Mol. Biol.* **190,** 593–604
31. Brünger, A. T., Adams, P. D., Clore, G. M., DeLano, W. L., Gros, P., Grosse-Kunstleve, R. W., Jiang, J.-S., Kuszewski, J., Nilges, M., Pannu, N. S., Read, R. J., Rice, L. M., Simonson, T., and Warren, G. L. (1998) *Acta Crystallogr. Sect. D Biol. Crystallogr.* **54,** 905–921
32. Wikstrom, M., Drakenberg, T., Forsen, S., Sjobring, U., and Bjorck, L. (1994) *Biochemistry* **33,** 14011–14017
33. O'Neill, J. W., Kim, D. E., Baker, D., and Zhang, K. Y. (2001) *Acta Crystallogr. Sect. D Biol. Crystallogr.* **57,** 480–487
34. Laskowski, R. A., MacArthur, M. W., Moss, D. S., and Thornton, J. M. (1993) *J. Appl. Crystallogr.* **26,** 283–291
35. Bailey, S. (1994) *Acta Crystallogr. Sect. D Biol. Crystallogr.* **50,** 760–763
36. McDonald, I. K., and Thornton, J. M. (1994) *J. Mol. Biol.* **238,** 777–793
37. Wikstrom, M., Forsen, S., and Drakenberg, T. (1996) *Eur. J. Biochem.* **235,** 543–548
38. Pervushin, K., Riek, R., Wider, G., and Wuthrich, K. (1997) *Proc. Natl. Acad. Sci. U. S. A.* **94,** 12366–12371
39. Genovese, A., Bouvet, J. P., Florio, G., Lamparter-Schummert, B., Bjorck, L., and Marone, G. (2000) *Infect. Immun.* **68,** 5517–5524
40. Philo, J. S., Aoki, K. H., Arakawa, T., Narhi, L. O., and Wen, J. (1996) *Biochemistry* **35,** 1681–1691
41. Livnah, O., Johnson, D. L., Stura, E. A., Farrell, F. X., Barbone, F. P., You, Y., Liu, K. D., Goldsmith, M. A., He, W., Krause, C. D., Pestka, S., Jolliffe, L. K., and Wilson, I. A. (1998) *Nat. Struct. Biol.* **5,** 993–1004